Analytical Modeling of Electromigration Failure for VLSI Interconnect Tree Considering Temperature and Segment Length Effects

Hai-Bao Chen, *Member, IEEE*, Sheldon X.-D. Tan, *Senior Member, IEEE*, Jiangtao Peng, Taeyoung Kim, *Student Member, IEEE*, and Jie Chen, *Fellow, IEEE*

***Abstract*—Electromigration (EM) is a major concern for very large-scale integration (VLSI) interconnect reliability, particularly for interconnect trees with multibranch metal wires representing continuously connected metal (Cu) lines terminated at diffusion barriers. For EM modeling and assessment, one important problem is to perform fast EM time to failure analysis for practical VLSI chips. Compact modeling for EM effects for the interconnect tree has been studied recently to better EM signoff analysis. But the existing method cannot consider wires stressed under time-varying temperature, which is very typical for practical chip working conditions. In this paper, we develop the exact analytic model for the stress evolution of interconnect trees under different current density and varying segment length from the first principle. Due to the difficulty in obtaining the exact analytical solution, we focus on three-terminal wire in this paper. The stress evolution is modeled by two Korhonen's equations coupled through boundary conditions which are solved with the Laplace transformation technique. The new analytical EM model is further extended to consider the time-varying temperature stressing condition and initial non-zero residual stress. The proposed method is compared with the finite-element method (FEM) tool COMSOL, the recently proposed eigenfunction-based method, and the published EM simulator XSim. The comparison shows that the analytical solution agrees well with the results from the FEM numerical analysis. It uses much fewer terms compared to the eigenfunction method for the same accuracy. It also agrees very well with XSim, which is consistent with the previously reported measured results.**

***Index Terms*—Electromigration reliability, stress evolution, three-terminal interconnect tree, segment length, time-varying temperature.**

Manuscript received May 6, 2017; revised July 29, 2017; accepted August 21, 2017. Date of publication August 30, 2017; date of current version December 7, 2017. This work was supported in part by the Nature Science Foundation of China under Grant 61604095, in part by the 985 Research Fund from Shanghai Jiao Tong University, in part by NSF under Grant CCF-1527324, and in part by Hong Kong RGC under Project Cityu 111613. *(Corresponding author: Hai-Bao Chen.)*

H.-B. Chen and J. Peng are with the Department of Micro/Nano-Electronics, Shanghai Jiao Tong University, Shanghai 200240, China (e-mail: haibaochen@sjtu.edu.cn; pjt_nina@sjtu.edu.cn).

S. X.-D. Tan and T. Kim are with the Department of Electrical and Computer Engineering, University of California at Riverside, Riverside, CA 92521 USA (e-mail: stan@ece.ucr.edu; tkim049@cs.ucr.edu).

J. Chen is with the Department of Electronic Engineering, City University of Hong Kong, Hong Kong, China (e-mail: jichen@cityu.edu.hk).

Color versions of one or more of the figures in this paper are available online at http://ieeexplore.ieee.org.

Digital Object Identifier 10.1109/TDMR.2017.2746660

I. Introduction

As THE performance of present day integrated circuits increases, electromigration (EM) has become a major reliability concern for current and future VLSI technologies [1]–[3]. International Technology Roadmap for Semiconductors (ITRS) 2014 predicts that the lifetime of wires due to EM will decrease by half for each new generation as shown in Fig. 1, which shows the actual and predicted ones of lifetime scaling versus interconnect geometry [4]. It is important to be able to assess the EM reliability of three-terminal interconnect trees since a layout-design of integrated circuits often has interconnects with junctions. More accurate analytical modeling and analysis techniques are required for the prediction of lifetime based on the stress evolution equation.

An interconnect tree is often bounded by diffusion barriers at vias and contacts in VLSI chips. In the general case, an interconnect tree has more than one terminal branch when the junctions are included [5], [6]. Instead of studying interconnect reliability of trees, most work of interconnect reliability in the literature focuses on simple straight lines that only have two terminals. For the multi-branch interconnect tree, the stress evolution in the void nucleation phase during EM is a complex function of the line length of each wire segment, the current density and the temperature. In conventional interconnect reliability assessment approaches, interconnect trees are broken into a number of segments and then the reliability of the corresponding segments are independently calculated.

The EM behaviors of multi-branch interconnect trees for the void nucleation phase are still governed by the Korhonen's equation [7]. The mathematical problem corresponding to the reliability calculations of interconnect trees is extremely difficult to solve, but once the interconnect tree is broken into many simple single-segment wires, the Korhonen's equation can be applied to modeling stress evolution process for each segment. There are multiple valid reliability assessment approaches for complex shape of interconnect trees - only the solution of the Korhonen's equation for the straight line segment with two terminals needs to be found. The stress value for multi-branch interconnect trees must be continuous at the borders of two connected segments. Also, the atomic flux must be continuous at the borders in the case of equal segment widths, which is analyzed below. The current densities at the boundaries of interconnect trees may not be continuous but the currents for every wire segment must meet the Kirchhoff's circuit law.

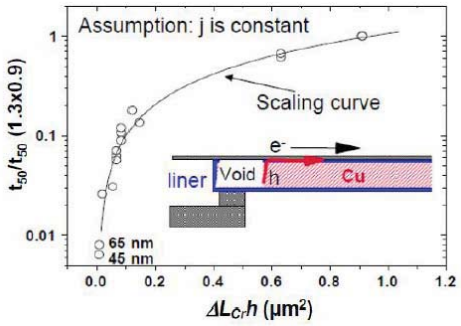

Fig. 1. The lifetime of interconnect wires versus technology nodes by ITRS2014 [4].

The lifetime of EM failure mechanisms decreases exponentially with temperature [8]. This can be seen most clearly from the semi-empirical Black's equation [9]:

$$MTTF = Aj^{-n}exp\{E_a/kT\}, \tag{1}$$

which calculates mean time-to-failure (MTTF) based on known current densities (j) and temperatures (T). In (1), k is the Boltzmann's constant, E_a is the EM activation energy. The symbol A is a constant, which depends on a number of factors, including grain size, line structure and geometry, current density, thermal history, etc. The current density exponent n is found by fitting the model to experimental data. The exact number of n is very debatable. The common understanding is that n is close to 1 when the growth phase is dominant, while n is close to 2 when the nucleation phase is dominant in the EM failure process [10]–[12]. Practically, n in Black's equation commonly was found between 1 and 2 as it models the two EM failure processes together, and n was affected by the critical current density or the critical stress of the wires [13]. Recent study shows that n actually is close to 1 in copper damascene wires with EM sink and reservoir structures [13]–[15]. As a result, the application of the Black's equation on today's interconnects such as a large variety of circuit-like structures may lead to significant errors in the lifetime prediction [16], [17]. In addition, for high performance multi-core and emerging 3D microprocessors, dynamic reliability management has been merged to maximize system performance under life time constraints [18]–[20]. Existing EM model is difficult to use as it cannot tell the reliability impacts caused by the dynamic temperature changes over time. Recently some more EM models have been proposed to mitigate some of those mentioned problems [21]–[23]. However, these models are still based on the Korhonen's equation for calculating lifetime prediction of each time period with constant temperature. As a result, a dynamic EM model considering time-varying temperature conditions is very desirable for system level reliability management.

Many research attempts have been spent to derive exact and approximate mathematical models for the electromigration nucleation process for a single, straight-line structure investigated in reliability analysis. However, obtaining analytical solutions for electromigration-induced stress evolution in general interconnect structure are extremely difficult (if not impossible). Korhonen, for example, developed an analytical model for straight-line interconnects under the assumptions of constant temperature and current density [7]. For more complex VLSI interconnect trees such as circuit-like interconnects with multi segments [13]–[15], conservative analytic modes are needed to analyze mechanical stress evolution during electromigration.

Also, a new technique for EM assessment in power delivery networks of VLSI systems has been reported in [24] and [25]. However, it did not give an accurate analytic form to model an multi-segment interconnect tree. Analytic model for describing stress evolution process of multi-branch interconnect tree have been studied in [26] and [27], but this new analytic model needs to assume that each wire segment in the interconnect tree has the same length. Analytic model for multi-branch tree with different lengths of wire segments is still unsolved problem. In [26] and [27], a Laplace transform based method has been proposed for analytic modeling and analysis of the straight-line 3-terminal wires, the T-shaped 4-terminal wires and the cross-shaped 5-terminal wires, which assumes that each wire segment in the interconnect tree has the same length. The EM behavior of three-terminal Cu interconnect trees were described in [28] and [29] and the effects of different current density and segment length in a three-terminal interconnect were experimentally studied. But they did not provide accurate analytical modeling and analysis techniques for three-terminal interconnect trees in which the wire segments had various finite lengths and did not consider the effects of time-varying temperatures on the calculation of stress evolution by electromigration.

In this work, we develop the analytic model for stress evolutions of interconnect tree wires with varying wire segment lengths under time-varying temperature stressing conditions. This new method first solves the stress evolution equation (Korhonen's equation) considering different current density and varying segment length in three-terminal interconnect tree by decoupling the individual segments through the boundary conditions. The resulting equations are then solved with the Laplace transformation technique and the analytical solution can be represented by a set of auxiliary basis functions using the known complementary error function. The evolutions of tensile and compressive stresses are simulated for several cases with different current densities and segment lengths. Furthermore, the new analytical EM model is further extended to consider time-varying temperature stressing condition and initial non-zero residual stress.The simulation results are compared with the finite element tool COMSOL, which shows that the analytical solution agrees well with the numerical analysis results. We also compared the new method with the published EM simulator XSim [30], which is consistent with the previously reported measured results, and recently proposed eigenfunction method [31]. The new method agrees with XSim very well for the three-terminal wires. Compared with the eigenfunction method, the proposed method uses much fewer terms to achieve the same accuracy (better convergence).

The rest of this article is organized as follows. Section II will present the basic Korhonen's equation describing the hydrostatic stress in a single confined metal line with blocking boundary conditions for the void nucleation phase.

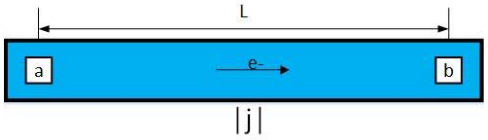

Fig. 2. The single straight-line metal wire.

In Section III, we will present our analytical solution of the stress evolution equation by using the Laplace transformation technique for three-terminal interconnect tree with various wire segment lengths. The effects of different current density and segment length configurations on stress evolution will also be considered in Section III. In Section IV, we will propose a dynamic EM-induced stress model which can be used to calculate the stress values under any time-varying temperature profile. In Section V, experimental and simulation testing of a number of benchmark examples will be performed to verify the effectiveness of the proposed analytic model. Concluding remarks will be drawn in Section VI.

II. Korhonen's Equation for a Single Metal Wire

Before we present our analytic model for three-terminal interconnect tree, we first review the basic Korhonen's equation describing the hydrostatic stress in a single confined metal line with blocking boundary conditions (BC) and given initial conditions (IC), and briefly discuss how the void nucleation time is approximated from the analytic solution to the Korhonen's equation.

Fig. 2 shows a single metal wire with two terminals "a" and "b". For the void nucleation phase during EM, the tensile stress will be developed over time at the cathode node ("a") where the atoms deplete and the compressive stress will be developed at the anode node ("b") where the atoms accumulate. The build-up stress gradient leads to a mechanical driving force which opposes the electromigration wind force. It was agreed that a void starts to nucleate at the cathode end of an interconnect line when the tensile stress reaches the so-called critical stress, σ_{crit}, which should be used as a condition for a void nucleation.

The classical model of the homogeneous nucleation, [32], says that a cavity located in the metal, loaded with the hydrostatic tensile stress σ, can either shrink or enlarge depending on the original cavity size R. In the very rough approximation, which we use for illustrative purposes, if $R < R_c = 2\gamma/\sigma$, where γ is the cavity surface energy per unit area, the cavity will shrink to reduce the free energy of the system represented by the metal with cavity, if $R > R_c$, the cavity will enlarge to reduce this energy. Thus, assuming that the preexisting cavities are of the $5-10nm$ size, we can estimate the critical stress level of $\sigma \approx 200 \sim 500MPa$ when $\gamma = 1N/m^2$. If the atomic diffusion stops before the tensile stress reaches the critical stress value, the interconnect wires will become immortal.

The electromigration depletes the atoms by driving them to the anode "b", which generates a stress σ that opposes the electromigration flux. For a single interconnect line shown in Fig. 2, the stress change in the metal is well described by Korhonen's equation [7]:

$$\frac{\partial \sigma(x,t)}{\partial t} = \frac{\partial}{\partial x}\left[\kappa\left(\frac{\partial \sigma(x,t)}{\partial x} + G\right)\right], \tag{2}$$

where κ is the stress diffusivity and G is the EM driving force. For practical interconnect wires, the terms κ and G can be computed as follows

$$\kappa = \frac{D_a B \Omega}{kT},\ G = \frac{Eq}{\Omega},$$

where D_a is the effective atomic diffusivity, B is the effective bulk modulus, Ω is the atomic volume, k is Boltzmann's constant, T is the absolute temperature, E is the electric field, and q is the effective charge. It should be noted that E can be calculated by $E = \rho j$ where ρ is the resistivity and j is the current density, and q can be replaced by a known quantity $q = |Z|e$ where Z is the effective charge number and e is the elementary charge. Thus, the driving force G can be calculated by $G = \frac{\rho j |Z| e}{\Omega}$.

The effective atomic diffusion D_a is determined mainly by the interfacial and grain boundary diffusivities which can be characterized by the grain microstructure development in the interconnect line [33], [34]. A portion with the smaller grain size is characterized by a higher diffusivity. Indeed, the effective D_a can be represented by the volume averaged characteristics of the interconnect line characterized by the presence of grain boundary and interfaces [35]. Traditionally people average grain size for the whole interconnect line for considering electromigration failure [6], [22], [34]. If the material transport along the line is assumed to be affected only by the grain boundary diffusion, the atomic diffusion coefficient D_a can be calculated by $D_a = wD_{GB}/d$ where w is the grain boundary width, D_{GB} is the grain boundary diffusion coefficient and d is the grain size [7], [36]. If the information about distribution of the micrograniular segments in the almost bamboo line is available, then it can be taken into account. Korhonen's model is widely used to analyze electromigration induced failures in near-bamboo lines. The advantage of this model is that a closed-form expression for stress evolution can be obtained during electromigration [36]. It should also be mentioned that the effective atomic diffusion coefficient D_a can be replaced by the well-known Arrhenius equation $D_a = D_0 \exp(-\frac{E_a}{kT})$, where D_0 is the pre-exponential factor and E_a is the activation energy [23], [35]. The values of the parameters used for modeling and simulations throughout this paper were set to $\rho = 3e-8\Omega \cdot m$, resistivity of Cu, $\Omega = 8.78e-30m^3$, $e = 1.60e-19C$, $k = 1.38e-23J/K$, $B = 1e11Pa$, $D_0 = 5.2e-5m^2/s$, $E_a = 1.1eV$, and $Z = 10$. These parameters were chosen according to [26] and [35].

Korhonen's equation (2) is formally very similar to the familiar diffusion equation (a partial differential equation) with the diffusivity-like parameter κ. Throughout the rest of the paper, let us assume that the stress diffusivity κ does not depend on the time, i.e., κ is a constant value. We can find the closed-form solutions of Korhonen's equation with different BC for several electromigration problems based on the Laplace transform technique. For the blocking BC during

the void nucleation phase, the atomic fluxes are blocked at both the ends "a" and "b", i.e., $\frac{D_a}{\Omega kT}(\frac{\partial\sigma(x,t)}{\partial x}+G)|_{x=0,L}=0$. Following [7], the closed-form expression for the stress evolution equation in the single interconnect wire can be described as follows

$$\sigma(x,t,\kappa,G)=\sigma_T+GL\left\{\frac{1}{2}-\frac{x}{L}-4\sum_{n=0}^{\infty}\times\frac{\cos\left((2n+1)\pi\frac{x}{L}\right)}{(2n+1)^2\pi^2\exp\left((2n+1)^2\pi^2\frac{\kappa t}{L^2}\right)}\right\},\tag{3}$$

where σ_T is the pre-existing residual stress. Based on Korhonen's equation, an analytical model for estimating the EM reliability of the single metal wire can be obtained, which is based on calculation of the lifetime of the cathode node "a" in the wire by estimating the time to void nucleation. If the tensile stress at the cathode node "a" reaches the critical stress value [11], a void starts to nucleate at the cathode. To obtain an analytical expression for calculating the void nucleation time, we can just keep only one-term approximation ($n=0$) of the exact series solution (3) for the stress at the end $x=0$:

$$\sigma(t,T,j)\approx\sigma_T+GL\left(\frac{1}{2}-\frac{1}{2\exp\left\{\frac{D_aB\Omega t}{L^2kT}\right\}}\right).\tag{4}$$

By using the relationship $\sigma(t_{nuc},T,j)=\sigma_{crit}$, the void nucleation time t_{nuc} can be computed by the following analytic form [21], [24]

$$t_{nuc}=\frac{L^2kT}{D_aB\Omega}\ln\left\{\frac{\frac{\rho j|Z^*|eL}{2\Omega}}{\sigma_T+\frac{\rho j|Z^*|eL}{2\Omega}-\sigma_{crit}}\right\}.\tag{5}$$

It can be seen from (5) that the void nucleation time t_{nuc} depends on the critical tensile stress σ_{crit} which is not included in the Black's equation (1). For a single metal wire with length L, the critical tensile stress σ_{crit} can be calculated by $\sigma_{crit}=\frac{\rho j_{crit}|Z|eL}{2\Omega}$ [13], where j_{crit} is the critical current density. As a result, the void nucleation time is related to the critical current density, which is also not included in the Black's equation (1). The absence of mechanical stress evolution analysis can have serious effects on reliability of VLSI circuits such as circuit-like interconnects, typically resulting in significantly overestimating failure times, [7], [36]. In addition, this formula (5) for computing the void nucleation time is not logically valid when we consider time-varying temperature effects on the stress evolution process. If time-varying temperature conditions are considered for calculating the void nucleation time, there is a severe discrepancy between the actual and average temperature models [22]. We will also illustrate this point later in Section IV for three-terminal interconnect tree.

III. Accurate Analytic Model for Three-Terminal Interconnect Tree

In this section, we will develop an exact analytical model that can be applied to study the electromigration induced reliability of three-terminal interconnect tree with various wire segment lengths during the void nucleation phase. The effects of current density and segment length configurations on stress evolution at the void nucleation phase will be considered for this type of interconnect tree by the present analytical model.

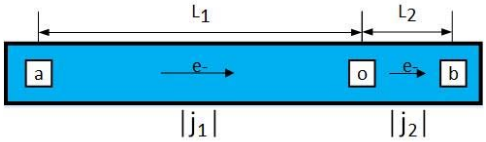

Fig. 3. Three-terminal interconnect tree with two wire segments.

A. Analytic Model for Stress Evolution Process

We now develop an exact closed-form solution for the EM-induced stress analysis of a three-terminal interconnect tree with two wire segments with different segment lengths as showed in Fig. 3. The two segments which are interacted by the rest of the circuit may not have the same current density. For this three-terminal interconnect tree with two wire segments, the following two partial differential equations based on Korhonen model [7] can be used to describe the stress evolution process in the two wire segments:

$$\begin{aligned}&\frac{\partial\sigma_1(x,t)}{\partial t}=\frac{\partial}{\partial x}\left[\kappa_1\left(\frac{\partial\sigma_1(x,t)}{\partial x}+G_1\right)\right],\ -L_1<x<0,\ t>0,\\&\frac{\partial\sigma_2(x,t)}{\partial t}=\frac{\partial}{\partial x}\left[\kappa_2\left(\frac{\partial\sigma_2(x,t)}{\partial x}+G_2\right)\right],\ 0<x<L_2,\ t>0.\end{aligned}\tag{6}$$

The equations (6) are formally very similar to the familiar partial differential equation for diffusion with the diffusivities κ_1 and κ_2 replacing the conventional diffusion coefficients. For the sake of simplicity, we need to assume that each segment in the three-terminal interconnect tree has the same diffusivity, that is, $\kappa_1=\kappa_2=\kappa$. In order to ensure that this assumption is met, the temperature for each segment should be kept the same due to the fact that the diffusion coefficient in metal (Cu) lines depends on the temperature.

For the void nucleation phase, we need to consider the case of the three-terminal interconnect tree where the atom flux is blocked at both ends, that is, $\frac{D_a}{\Omega kT}(\frac{\partial\sigma(x,t)}{\partial x}+G)|_{x=-L_1,L_2}=0$. The stresses in the two wire segments will interfere with each other, which can be reflected in the stress value at the intersection "o". The BC of the equations (6) for the void nucleation phase are then found to be

$$\begin{aligned}&\kappa_1\left(\frac{\partial\sigma_1(x,t)}{\partial x}+G_1\right)=0,\ \texttt{at}\ x=-L_1,\ t>0,\\&\sigma_1(x,t)=\sigma_2(x,t),\ \texttt{at}\ x=0,\ t>0,\\&\kappa_1\left(\frac{\partial\sigma_1(x,t)}{\partial x}+G_1\right)=\kappa_2\left(\frac{\partial\sigma_2(x,t)}{\partial x}+G_2\right),\\&\qquad\qquad\texttt{at}\ x=0,\ t>0,\\&\kappa_2\left(\frac{\partial\sigma_2(x,t)}{\partial x}+G_2\right)=0,\ \texttt{at}\ x=L_2,\ t>0.\end{aligned}\tag{7}$$

The first and fourth equations in (7) imply that blocking boundary conditions for the void nucleation phase are required,

such that the atom fluxes are zero at both the ends. The second equation in (7) ensures that stresses at the intersection point of the two wire segments are continuous. The third equation in (7) means that the atomic fluxes are also continuous at the intersection. To obtain the analytical solution of (7), we assume that the initial conditions (IC) are given by:

$$\begin{aligned}\sigma_1(x,0) &= 0,\ -L_1 < x < 0,\\ \sigma_2(x,0) &= 0,\ 0 < x < L_2,\end{aligned} \tag{8}$$

which means that there is no stress everywhere in each line segment at $t = 0$. The IC for stress evolution is that there is no driving force for the sink or source reactions when electromigration in the void nucleation phase starts.

With the BC (7) and the IC (8), we consider the exact time-dependent solutions for the equations (6) by the Laplace transform technique. For $t \geq 0$, the Laplace transform of the function $\sigma_i(x,t)$ $(i = 1,2)$ is defined by $\hat{\sigma}_i(x,s) = \int_0^{+\infty} e^{-st}\sigma_i(x,t)dt$. Instead of solving directly for $\sigma_i(x,t)$, we derive new equations for $\hat{\sigma}_i(x,s)$. Once we find $\hat{\sigma}_i(x,s)$, we use inverse transform to determine $\sigma_i(x,t)$. The first step is to take the Laplace transform of both sides of the original partial differential equations (6) with the IC (8). Hence, we obtain the ordinary differential equations

$$\begin{aligned}\frac{d^2\hat{\sigma}_1(x,s)}{dx^2} &= \frac{s}{\kappa_1}\hat{\sigma}_1(x,s),\ -L_1 < x < 0,\\ \frac{d^2\hat{\sigma}_2(x,s)}{dx^2} &= \frac{s}{\kappa_2}\hat{\sigma}_2(x,s),\ 0 < x < L_2.\end{aligned} \tag{9}$$

The particular solutions can be determined using variation of parameters or the method of undetermined coefficients. Solving for $\hat{\sigma}_i(x,s)$ in (9), we have

$$\begin{aligned}\hat{\sigma}_1(x,s) &= A_1 e^{\sqrt{\frac{s}{\kappa_1}}x} + B_1 e^{-\sqrt{\frac{s}{\kappa_1}}x},\\ \hat{\sigma}_2(x,s) &= A_2 e^{\sqrt{\frac{s}{\kappa_2}}x} + B_2 e^{-\sqrt{\frac{s}{\kappa_2}}x},\end{aligned} \tag{10}$$

where the coefficients A_1, A_2, B_1, and B_2 are determined by the BC (7). In order to obtain the undetermined coefficients, we need to take the Laplace transform for the BC (7):

$$\begin{aligned}&\frac{d\hat{\sigma}_1(x,s)}{dx} + \frac{G_1}{s} = 0,\ \texttt{at}\ x = -L_1,\\ &\hat{\sigma}_1(x,s) = \hat{\sigma}_2(x,s),\ \texttt{at}\ x = 0,\\ &\kappa_1\left(\frac{d\hat{\sigma}_1(x,s)}{dx} + \frac{G_1}{s}\right) = \kappa_2\left(\frac{d\hat{\sigma}_2(x,s)}{dx} + \frac{G_2}{s}\right),\ \texttt{at}\ x = 0,\\ &\frac{d\hat{\sigma}_2(x,s)}{dx} + \frac{G_2}{s} = 0,\ \texttt{at}\ x = L_2.\end{aligned} \tag{11}$$

Substituting the expressions $\hat{\sigma}_1(x,s)$ and $\hat{\sigma}_2(x,s)$ from (10) into (11), we obtain the following linear system

$$\begin{bmatrix} \frac{a}{d_1} & -ad_1 & 0 & 0\\ 0 & 0 & ad_2 & -\frac{a}{d_2}\\ a & -a & -a & a\\ 1 & 1 & -1 & -1\end{bmatrix}\begin{bmatrix} A_1\\ B_1\\ A_2\\ B_2\end{bmatrix} = \begin{bmatrix} -c_1\\ -c_2\\ c_2 - c_1\\ 0\end{bmatrix}, \tag{12}$$

where $a = \sqrt{\frac{s}{\kappa}}$, $c_i = \frac{G_i}{s}$, and $d_i = e^{\sqrt{\frac{s}{\kappa}}L_i}(i = 1,2)$. Solution of the linear system (12) yields these coefficients:

$$A_1 = \frac{-2c_1d_1^{-1}d_2^{-2} + (c_1 - c_2)d_2^{-2} + 2c_2d_2^{-1} + (c_1 - c_2)}{-2a\left(1 - d_1^{-2}d_2^{-2}\right)},$$

$$B_1 = \frac{(c_1 - c_2)d_1^{-2}d_2^{-2} + 2c_2d_1^{-2}d_2^{-1} + (c_1 - c_2)d_1^{-2} - 2c_1d_1^{-1}}{-2a\left(1 - d_1^{-2}d_2^{-2}\right)},$$

$$A_2 = \frac{(c_1 - c_2)d_1^{-2}d_2^{-2} - 2c_1d_1^{-1}d_2^{-2} + (c_1 - c_2)d_2^{-2} + 2c_2d_2^{-1}}{-2a\left(1 - d_1^{-2}d_2^{-2}\right)},$$

$$B_2 = \frac{2c_2d_1^{-2}d_2^{-1} + (c_1 - c_2)d_1^{-2} - 2c_1d_1^{-1} + (c_1 - c_2)}{-2a\left(1 - d_1^{-2}d_2^{-2}\right)}. \tag{13}$$

An analytical method based on the Laplace transform technique has been developed for the EM-induced stress evolution problem of the three-terminal interconnect tree, when the IC (8) are given and the BC (7) are known at the three terminals. On the basis of these known coefficients A_i and B_i, the closed form solution can be determined from (10) for each segment by using the inverse Laplace transform technique. In order to derive the analytical solutions $\sigma_1(x,t)$ and $\sigma_2(x,t)$, we will start by introducing the notations:

$$\begin{aligned}\xi_1(x,n) &= (2n+1)L_1 + (2n+2)L_2 - x,\\ \xi_2(x,n) &= (2n)L_1 + (2n+2)L_2 - x,\\ \xi_3(x,n) &= (2n)L_1 + (2n+1)L_2 - x,\\ \xi_4(x,n) &= (2n)L_1 + (2n)L_2 - x,\\ \xi_5(x,n) &= (2n+2)L_1 + (2n+2)L_2 + x,\\ \xi_6(x,n) &= (2n+2)L_1 + (2n+1)L_2 + x,\\ \xi_7(x,n) &= (2n+2)L_1 + (2n)L_2 + x,\\ \xi_8(x,n) &= (2n+1)L_1 + (2n)L_2 + x,\\ \eta_1(x,n) &= (2n+2)L_1 + (2n+2)L_2 - x,\\ \eta_2(x,n) &= \xi_1(x,n),\ \eta_3(x,n) = \xi_2(x,n),\\ \eta_4(x,n) &= \xi_3(x,n),\ \eta_5(x,n) = \xi_6(x,n),\\ \eta_6(x,n) &= \xi_7(x,n),\ \eta_7(x,n) = \xi_8(x,n),\\ \eta_8(x,n) &= (2n)L_1 + (2n)L_2 + x,\end{aligned} \tag{14}$$

where x is a location in the three-terminal interconnect tree and n is a nonnegative integer. These functions ξ_i and $\eta_i(i = 1,2,\ldots,8)$ are previously determined from the location x and the nonnegative integer n. Also we need to introduce the complementary error function which is defined as $\texttt{erfc}\{x\} = \frac{2}{\sqrt{\pi}}\int_x^{+\infty} e^{-t^2}dt$. In mathematics, the complementary error function is a special function that can be used in probability, statistics, and partial differential equations describing diffusion. Based on the complementary error function, we construct the following basis function

$$g(x,t) = 2\sqrt{\frac{\kappa t}{\pi}}e^{-\frac{x^2}{4\kappa t}} - x \times \texttt{erfc}\left\{\frac{x}{2\sqrt{\kappa t}}\right\}. \tag{15}$$

It would be necessary to say why the basis function shown in (15) is adopted instead of a trigonometric function in terms of location and time for calculating the analytical solution for each segment in the three-terminal interconnect tree. The reason is that a general solution for the stress evolution equation for this tree type is provided in a functional form of $g(x,t)$. By using these functions $\xi_i(x,n)$, $\eta_i(x,n)$ and $g(x,t)$, we can obtain the exact analytical solutions for the stress evolution in

both segments:

$$\sigma_1(x,t) = -\frac{1}{2}\sum_{n=0}^{+\infty}\{-2G_1 g(\xi_1,t) + (G_1-G_2)g(\xi_2,t) + 2G_2 g(\xi_3,t) + (G_1-G_2)g(\xi_4,t)\} - \frac{1}{2}\sum_{n=0}^{+\infty}\{(G_1-G_2)g(\xi_5,t) + 2G_2 g(\xi_6,t) + (G_1-G_2)g(\xi_7,t) - 2G_1 g(\xi_8,t)\}, \quad (16)$$

$$\sigma_2(x,t) = -\frac{1}{2}\sum_{n=0}^{+\infty}\{(G_1-G_2)g(\eta_1,t) - 2G_1 g(\eta_2,t) + (G_1-G_2)g(\eta_3,t) + 2G_2 g(\eta_4,t)\} - \frac{1}{2}\sum_{n=0}^{+\infty}\{2G_2 g(\eta_5,t) + (G_1-G_2)g(\eta_6,t) - 2G_1 g(\eta_7,t) + (G_1-G_2)g(\eta_8,t)\}. \quad (17)$$

It should be mentioned that the closed-form expressions $\sigma_1(x,t)$ in (16) and $\sigma_2(x,t)$ in (17) are obtained by assuming that the preexisting residual stress σ_T is zero. If we consider the effect of the residual stress σ_T preexisting in the interconnect line, by a direct derivation we can easily calculate the total stress $\sigma_{i,total}(x,t)(i=1,2)$ experienced by electromigration as the summation of the two stresses $\sigma_i(x,t)$ and σ_T, i.e.,

$$\sigma_{1,total}(x,t) = \sigma_1(x,t) + \sigma_{1,T},\ \sigma_{2,total}(x,t) = \sigma_2(x,t) + \sigma_{2,T}, \quad (18)$$

where $\sigma_{1,T}$ and $\sigma_{2,T}$ are the residual stresses preexisting in the left and right segments, respectively.

Obviously, the closed-form expressions (16) and (17) show exact series solutions of stress evolution equations for the two wire segments. When the tensile stress at the cathode end of an interconnect wire exceeds the critical stress σ_{crit} necessary for void nucleation, the value of the void nucleation time t_{nuc} can be extracted from the general expressions (16) and (17). Once a void starts to nucleate, it can grow to larger volume even spanning the whole interconnect line. On the other hand, an approximate value of t_{nuc} can be derived from the approximate solution of the one dimensional diffusion-like equation by using the first dominant term ($n=0$) approximation for each segment

$$\sigma_1(x,t) \approx -\frac{1}{2}\{-2G_1 g(\xi_1(x,0),t) + (G_1-G_2)g(\xi_2(x,0),t) + 2G_2 g(\xi_3(x,0),t) + (G_1-G_2)g(\xi_4(x,0),t)\} - \frac{1}{2}\{(G_1-G_2)g(\xi_5(x,0),t) + 2G_2 g(\xi_6(x,0),t) + (G_1-G_2)g(\xi_7(x,0),t) - 2G_1 g(\xi_8(x,0),t)\}, \quad (19)$$

$$\sigma_2(x,t) \approx -\frac{1}{2}\{(G_1-G_2)g(\eta_1(x,0),t) - 2G_1 g(\eta_2(x,0),t) + (G_1-G_2)g(\eta_3(x,0),t) + 2G_2 g(\eta_4(x,0),t)\} - \frac{1}{2}\{2G_2 g(\eta_5(x,0),t) + (G_1-G_2)g(\eta_6(x,0),t) - 2G_1 g(\eta_7(x,0),t) + (G_1-G_2)g(\eta_8(x,0),t)\}. \quad (20)$$

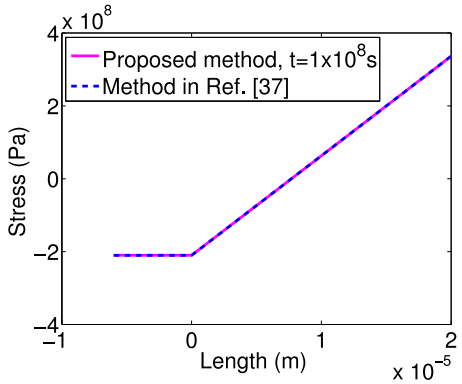

Fig. 4. Steady state stress distribution for an active segment of length $L_2 = 20\mu m$ with an inactive sink of length $L_1 = 6\mu m$.

Similar to the single wire case, the void nucleation time can be obtained by solving the equations

$$\sigma_1(x, t_{nuc,1}) = \sigma_{crit},\ \sigma_2(x, t_{nuc,2}) = \sigma_{crit}, \quad (21)$$

where the critical stress σ_{crit} is known. It can be seen from (19)-(21) that the void nucleation time depends on the critical tensile stress and hence is related to the critical current density which is not included in the Black's equation (1). Also, we can see from (19) and (20) that the lifetime is also affected by the segment length configuration information which has not been fully reflected in the Black's equation (1). The MTTF estimated by the Black's equation becomes invalid for this type of circuit-like interconnects with multi segments [13]–[15]. It should be noted that because of the nonlinearity properties of the functions $\sigma_1(x, t_{nuc,1})$ and $\sigma_2(x, t_{nuc,2})$, iterative methods can be used to calculate the void nucleation time.

It should also be noted that the one-term approximation (19)-(20) can be used to calculate the steady-state stress distribution along three-terminal interconnect tree. Theoretically the stresses $\sigma_{i,steady}(i=1,2)$ at steady state can be given by $\sigma_{i,steady} = \sigma_i(x,+\infty)$. In order to verify the accuracy of computing the steady state stress distribution using (19)-(20), we consider a three-terminal interconnect tree with active and inactive segments like the interconnect structure as shown in [37]. For practical simulation in our work, the lengths of inactive and active segments are set to be $L_1 = 6\mu m$ and $L_2 = 20\mu m$, respectively, and the corresponding current density values are assumed to be $j_1 = 0A/m^2$ and $j_2 = 5\times 10^9 A/m^2$. It can be seen from Fig. 4 that the steady state stress distribution, obtained by the proposed method, is consistent with the previously published method in [37].

B. Considering Varying Current Density

To simplify the discussion of the effects of current density configurations on the void nucleation phase for the three terminal interconnect tree and the EM-induced stress evolution in this type of tree, we will in this section assume that the two segments in this tree have the same length $L_1 = L_2 = 20\mu m$. We will simulate the effects of electromigration using our closed-form expression presented in Section III-A. The proposed analytical solver is based on a one-dimensional Korhonen model which has been modified to

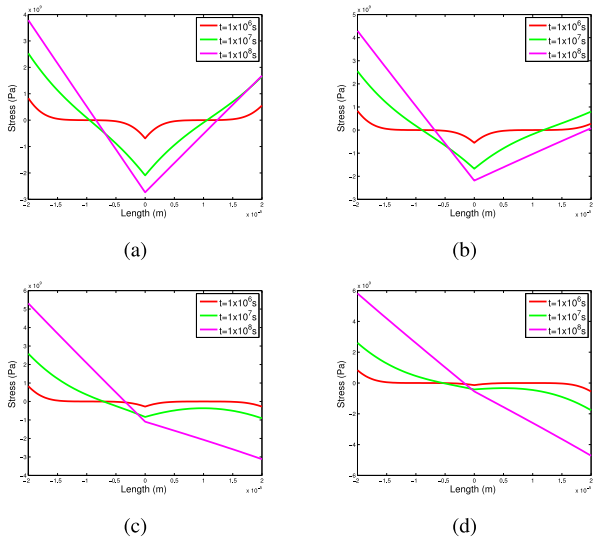

Fig. 5. The EM stress development along the segments 1 and 2 in the three-terminal interconnect tree: (a) $j_2 = -\frac{2}{3}j_1$; (b) $j_2 = -\frac{1}{3}j_1$; (c) $j_2 = \frac{1}{3}j_1$; (d) $j_2 = \frac{2}{3}j_1$.

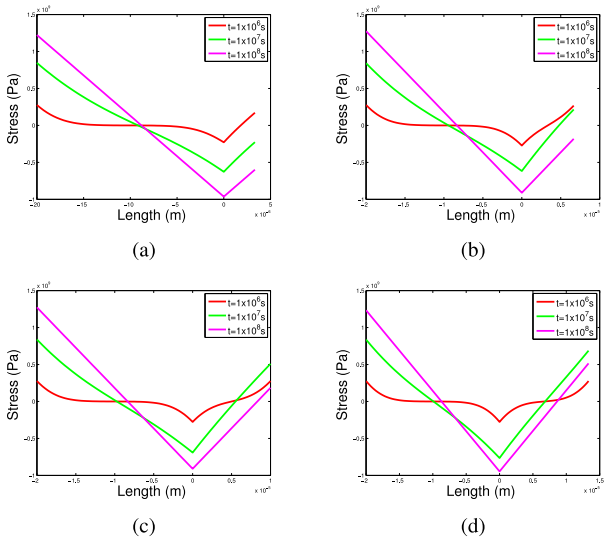

Fig. 6. The EM stress development along the segments 1 and 2 in the three-terminal interconnect tree: (a) $L_2 = \frac{1}{6}L_1$; (b) $L_2 = \frac{2}{6}L_1$; (c) $L_2 = \frac{3}{6}L_1$; (d) $L_2 = \frac{4}{6}L_1$.

account for a wide range of EM effects, including the impacts on the junction of the two wire segments. By the closed-form expressions, the stress evolution process can be modeled through initial prestress distribution to steady-state stress distribution. We can also model the associated void nucleation time using the proposed exact series solution when the tensile stress at the cathode end reaches the critical stress value.

Fig. 5 shows the four different current configurations that were used in tests of the three-terminal interconnect structure. A constant current density of $j_1 = 6 \times 10^{10} A/m^2$ was applied in the left line segment, while a current density with varying direction and magnitude, j_2, was used to stress the right line segment. For the cases (a) and (b), the currents have different directions that can lead to tensile stress at both ends of the two line segments. Voids can nucleate at the ends "a" and "b" of this interconnect tree when the tensile stresses exceed the critical stress necessary for void nucleation. It can be seen from Figs. 5(a) and 5(b) that the time-to-failure of the left line segment decreases as the current density in the right line segment decreases. However, the lifetime of the right line segment increases with the decrease of its current density. For the cases (c) and (d), the two segments have the same current direction. As a result, a tensile stress, which can cause voiding, develops at the cathode end "a" in the left line segment. Correspondingly, a compressive stress, which can cause metal extrusion, develops at the anode end "b" of the test structure. We can see from Figs. 5(c) and 5(d) that the compressive stress at the anode end increases as the current density of the right line segment increases for a fixed current density j_1 in the left line segment. The effect of current density on stress evolution is obvious in numerical simulation results obtained from the proposed analytical model, which fits well with the experimental work in [37].

C. Considering Varying Segment Length

In this section, the effects of segment length on lifetime at the void nucleation phase will be considered for the three-terminal interconnect tree. For simplicity (without loss of generality), we assume that the current densities j_1 and j_2 in the left and right segments are set to be $2 \times 10^{10} A/m^2$ and $-2 \times 10^{10} A/m^2$, respectively. Under this assumption, the directions of the currents in the two segments are opposite to each, which may cause tensile stress at both ends "a" and "b" under some given segment length configurations. The effect of electromigration on stress evolution will be simulated by using the proposed analytical model. Stress evolution, as presented in Section III-B, will be simulated through initial prestress distribution to a steady-state stress distribution. Also, the void nucleation time can be calculated for different segment length configurations by using the proposed closed-form expression.

The stress of a three-terminal interconnect tree as a function of its segment length configurations has been shown in (16)-(17). When this analytical model is applied to compute the lifetime of a three-terminal interconnect tree, it is obvious that the lifetime is changed as there is an increase or decrease in the segment length. The effect of segment length on lifetime has been demonstrated by experimental characterization with metallization technology [5]. However, it did not give a closed-form expression to model the three-terminal interconnect tree in which the neighboring segments interact with each other. In order to simulate the effect of segment length under the fixed current condition, we assume that the length of the left segment is $20\mu m$, and we will observe the change of stress by setting different current densities for the right segment. At the fixed current density configuration, it can be seen from Fig. 6 that the stress of the right segment decreases as the decrease of the length, which leads to the increase of the lifetime of the interconnect tree. This is due to the fact that the compressive stress developed at the node "o" of the test structure can interact with, and thus slow down the rate of tensile stress increase at the node "b". It was observed from Figs. 6(a) and 6(b) that a compressive hydrostatic stress can build up in the right segment when the length of this segment is small enough. They

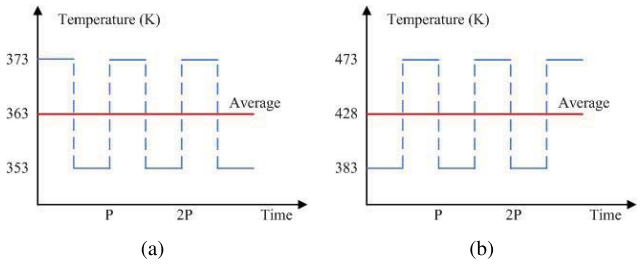

Fig. 7. The temperature profiles for simulations during the EM lifetime for the three-terminal interconnect tree: (a) temperatures between 353K and 373K; (b) temperatures between 383K and 473K.

demonstrate that the decreasing of the length of one of the segments taking place under the fixed electric current load results a progressive development of the compressive stress in this segment. This is caused by a continuously increasing back stress gradient in the short segment due to a continuous supply of atoms from the long segment to the segment border. On the other hand, as seen in Figs. 6(c) and 6(d), a tensile stress can also build up in the right segment if we increase the length of this segment. With the increase of the length of the right segment, a void can form at the node "b" of this segment where the tensile stress is the largest, resulting in simultaneous failure of the right segment. As a result, voids do not necessarily always form in the longest segment of an interconnect tree.

IV. Dynamic EM Modeling for Three-Terminal Interconnect Tree

The thermal effects have become a key factor in reliability-aware design under lifetime constraints. In this section, we will present a dynamic EM-induced stress model for three-terminal interconnect tree with various wire segment lengths, which can be used to calculate the stress values under any time-varying temperature profile for the EM-induced reliability.

A. Temperature Impacts on EM Effects

Black's model (1) needs to assume a constant temperature when applied to system-level thermal reliability analysis and design. This assumption eliminates the need for the thermal analysis on the interconnect lifetime prediction [22], [23]. When the interconnect trees have very high current densities ($j > 10^9 A/m^2$), thermal effects are becoming a limiting factor in high performance IC design due to the strong temperature dependence of reliability. Further, using average temperature is never a good practice for EM evaluation due to its Arrhenius nature $D_a = D_0 \exp(-\frac{E_a}{kT})$. If a constant temperature is considered in the stress evolution equation (6) for three terminal interconnect tree, it may result in pessimistic lifetime estimations in restricted design spaces.

As an example, we consider time-periodic responses of the interconnect temperature as shown in Figs. 7(a)–7(b) where P is the period. The current densities j_1 and j_2 in the left and right wire segments are set to be $1 \times 10^{10} A/m^2$ and $2 \times 10^{10} A/m^2$, respectively. Using the data from Fig. 7(a), the maximum and minimum temperatures in this three-terminal interconnect tree are assumed to be $373K$ and $353K$, respectively. Hence, the

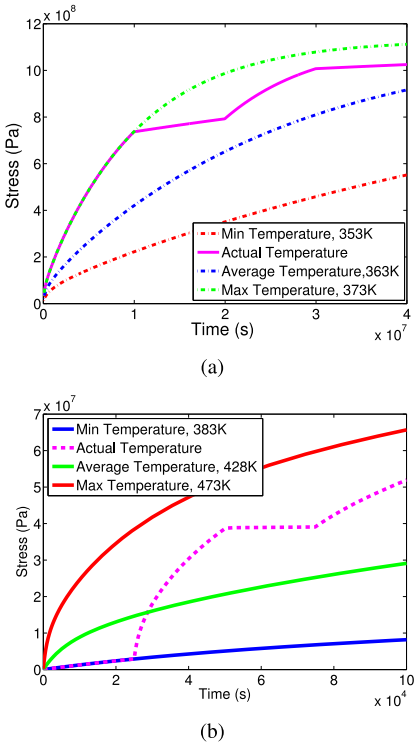

Fig. 8. The EM stress development at the cathode end of the three-terminal interconnect tree: (a) under temperature profiles shown in Fig. 7(a); (b) under temperature profiles shown in Fig. 7(b).

corresponding average temperature used for the simulation of stress evolution process is $363K$. Using these configurations, we can compare the values of stress obtained from the actual temperatures with those of the average, maximum, and minimum temperatures, and finally compare the time to the void nucleation by (21). A similar treatment can be required for the temperature profiles shown in Fig. 7(b).

Our simulation results are reported in Fig. 8 which shows four different cases where the temperatures profile affect the stress evolution process in the interconnect. In general, if the temperature change is within $10K$ and the current density is relatively small, using the average temperature for estimating interconnect lifetime is still a good approximation to the IC circuit designers. It can be observed from Fig. 8 that while the interconnect temperature variation increases (e.g., beyond $20K$), these differences become obvious by comparison between the actual and average temperatures. On the other hand, it can be seen from Fig. 8(a) that using the minimal temperature will make a big difference for stress calculations and it will lead to larger errors for interconnect lifetime prediction. Also, if we take the maximum temperature during the total simulation time, we can see from Fig. 8(b) that there is a serious difference between the actual and maximum stress profile calculations. Thus, the interconnect could be seriously underestimated, resulting in excessive design margin. Therefore, as the temperature variation increases, we can no longer use minimal/average/maximum temperature to estimate the interconnect reliability.

In view of the fact that the variation magnitude seriously affects the estimation of interconnect lifetime under

EM constraints, we will develop an exact dynamic EM-induced stress model for three-interconnect tree with various wire segment lengths in the next section. This dynamic model can be used for calculation of interconnect lifetime for any time-dependent temperature profile.

B. Dynamic EM Model Considering Varying Temperature

We now present dynamic EM modeling considering time-varying temperature for three-terminal interconnect trees with varying segment length. We start with the stress evolution equation as shown in (6) and assume that the two segments in the three-terminal interconnect tree have the same diffusivity. Considering that the temperature is time-dependent, we can re-write the diffusivities κ_1 and κ_2 as

$$\kappa_1(t) = \kappa_2(t) = \kappa(t) = \frac{D_0 \exp(-\frac{E_a}{kT(t)})B\Omega}{kT(t)}. \tag{22}$$

We still assume that the current density for each segment does not change over time. Therefore, the terms $G_1 = \frac{E_1 q}{\Omega}$ and $G_2 = \frac{E_2 q}{\Omega}$ are both constant.

We are now ready to derive the analytic solution of the stress evolution equation (6) with the time-varying temperature. Although we were able to use the Laplace transformation technique to obtain the series solution of stress evolution equation of three-terminal interconnect tree with various segment length and constant temperature, the stress evolution equation with time-varying temperature cannot be solved in a similar way. But fortunately, we have the following observations.

Theorem 1: Let $\sigma_i(x, t, \kappa_1)$ and $\sigma_i(x, t, \kappa_2)$ $(i = 1, 2)$ be the solutions to the stress evolution equation (6) with the diffusivities κ_1 and κ_2 for the same initial and boundary conditions, respectively, then we have

$$\sigma_i(x, t, \kappa_2) = \sigma_i\left(x, \frac{\kappa_2}{\kappa_1}t, \kappa_1\right).$$

Proof: This can be proved using the same technique as for the analogous result in [22]. Let $\tilde{\sigma}_i(x, t) = \sigma_i(x, \frac{\kappa_2}{\kappa_1}t, \kappa_1)$, then we just need to verify that $\tilde{\sigma}_i(x, t)$ is equal to $\sigma_i(x, t, \kappa_2)$. If we take the derivative of the partial derivative of $\tilde{\sigma}_i(x, t)$ with respect to t, then we can extract a partial differential equation (PDE), namely

$$\frac{\partial \tilde{\sigma}_i(x, t)}{\partial t} - \frac{\kappa_2}{\kappa_1}\frac{\partial \sigma_i\left(x, \frac{\kappa_2}{\kappa_1}t, \kappa_1\right)}{\partial t} = 0.$$

Since $\sigma_i(x, t, \kappa_1)$ is the solution of the equation (6) with the diffusivity κ_1 for certain initial and boundary conditions, we have $\frac{\partial \sigma_i(x, \frac{\kappa_2}{\kappa_1}t, \kappa_1)}{\partial t} = \frac{\partial}{\partial x}[\kappa_1(\frac{\partial \sigma_i(x, \frac{\kappa_2}{\kappa_1}t, \kappa_1)}{\partial x} + G_i)] = 0$. Substituting this expression into the above PDE, and noting that $\frac{\partial \tilde{\sigma}_i(x,t)}{\partial t} = \frac{\partial \sigma_i(x, \frac{\kappa_2}{\kappa_1}t, \kappa_1)}{\partial t}$, we have

$$\frac{\partial \tilde{\sigma}_i(x, t)}{\partial t} - \frac{\kappa_2}{\kappa_1}\frac{\partial}{\partial x}\left[\kappa_1\left(\frac{\partial \tilde{\sigma}_i(x, t)}{\partial x} + G_i\right)\right] = 0,$$

which implies that $\tilde{\sigma}_i(x, t)$ is the solution of the stress evolution equation (6) with the diffusivity κ_2 under the same initial and boundary conditions. This completes the proof of the theorem. ■

It can be seen from Theorem 1 that the stress evolution processes in the three-terminal interconnect tree are independent of the diffusivity in (6) which only affects the stress evolution speedup. This will lead to a time-shift invariant representation of the solution of the stress evolution equation with time-varying temperature based on the series solution (16)-(17) in the case of constant temperature. On the other hand, if we look at the complete analytic solution (16)-(17), only the term $g(x, t)$ is affected by the temperature $T(t)$. From (15) we can see that as long as $\kappa(T(t))t$ is constant, the basis function $g(x, t)$ will be the same. As a result, the temperature impact on the stress $\sigma_i(x, t, \kappa)$ through $\kappa(T(t))$ can be translated to the time period change for a three-terminal interconnect tree. In other words, a three-terminal interconnect tree whose stress development over a period Δt_2 under the temperature T_2 will be equal to the stress development for a three-terminal interconnect tree over a period $\frac{\kappa(T_2)}{\kappa(T_1)}\Delta t_2$ under the temperature T_1. Without loss of generality, we assume that the time period can be partitioned into n small segments:

$$\kappa(T(t)) = \begin{cases} \kappa_1, \ t \in [0, \ \Delta t_1], \\ \kappa_2, \ t \in (\Delta t_1, \ \Delta t_1 + \Delta t_2], \\ \cdots, \\ \kappa_n, \ t \in \left(\sum_{l=1}^{n-1} \Delta t_l, \ \sum_{l=1}^{i} \Delta t_l\right], \ n = 2, 3, \ldots. \end{cases} \tag{23}$$

Inside each time segment we assume that the temperature is constant, which leads to an invariant diffusivity for the stress evolution processes. As a result, the temperature-varying stress computation problem can be converted into the constant temperature problem.

Now we denote the dynamic stress with time-varying temperature by $\sigma_{i,th}(x, t, \kappa)$ for each metal wire. At the end of the first time segment $[0, \ \Delta t_1]$, we have $\sigma_{i,th}(x, \Delta t_1, \kappa_1) = \sigma_i(x, \Delta t_1, \kappa_1)$ where $\sigma_i(x, \Delta t_1, \kappa_1)$ is calculated by (16)-(17). Then at the current time $t_i = \sum_{l=1}^{i} \Delta t_l$, we have

$$\sigma_{i,th}\left(x, \sum_{l=1}^{n} \Delta t_l, \kappa_n\right) = \sigma_i\left(x, \sum_{l=1}^{n} \frac{\kappa_l}{\kappa_1}\Delta t_l, \kappa_1\right), \tag{24}$$

where $n = 1, 2, \ldots$, and $\sigma_i(x, t, \kappa)$ is given by (16)-(17). When the tensile stress (we ignore thermal residual σ_T for the time being for the sake of better presentation) reaches the critical stress σ_{crit}, a void will nucleate at the cathode end of a metal wire. If σ_{crit} is greater than the steady state tensile stress at the cathode end, no void will form and the wire is immortal. If the dynamic stress reaches a critical threshold at the i_{nuc}-th time segment, we have $\sigma_{crit} = \sigma_i(x, \sum_{l=1}^{n_{nuc}} \frac{\kappa_l}{\kappa_1}\Delta t_l, \kappa_1)$. Then the time to nucleation can be computed by $t_{nuc} = \sum_{l=1}^{n_{nuc}} \Delta t_l$.

V. Simulation Results and Discussions

The proposed dynamic EM model and the method of analysis of three-terminal interconnect tree with various wire segment lengths have been implemented in Matlab and compared with the finite element analysis tool COMSOL [38] and the electromigration simulator XSim [30] and the recently proposed eigenfunction method [31], which is considered as a "golden" tool in our work.

TABLE I
CURRENT DENSITY AND SEGMENT LENGTH CONFIGURATIONS USED FOR MODELING AND SIMULATION

Case	j_1	j_2	L_1	L_2
I	$1 \times 10^{10} A/m^2$	$5 \times 10^{9} A/m^2$	$10\mu m$	$20\mu m$
II	$1 \times 10^{10} A/m^2$	$1 \times 10^{9} A/m^2$	$10\mu m$	$20\mu m$
III	$1 \times 10^{10} A/m^2$	$0 A/m^2$	$10\mu m$	$20\mu m$
IV	$1 \times 10^{10} A/m^2$	$-5 \times 10^{9} A/m^2$	$6\mu m$	$20\mu m$
V	$1 \times 10^{10} A/m^2$	$-1 \times 10^{9} A/m^2$	$6\mu m$	$20\mu m$
VI	$1 \times 10^{10} A/m^2$	$0 A/m^2$	$6\mu m$	$20\mu m$

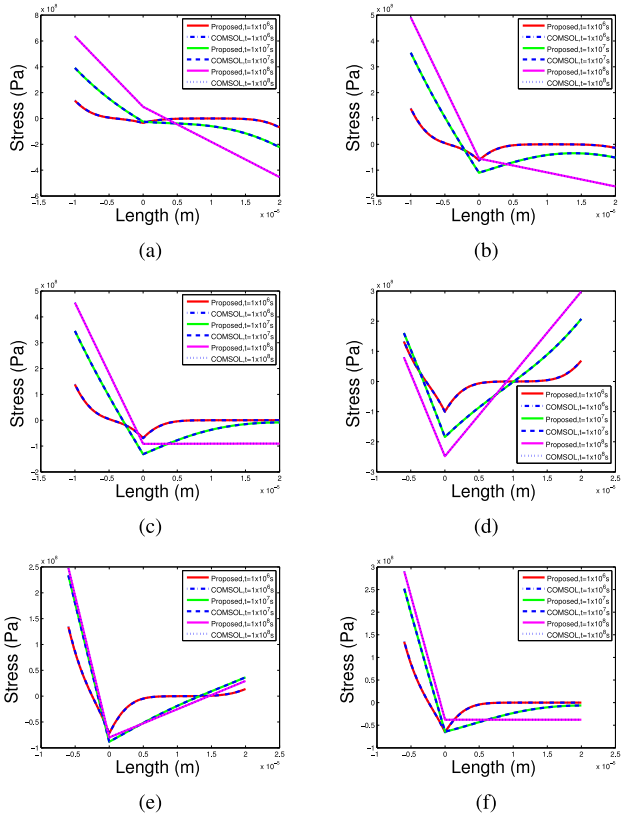

Fig. 9. The EM stress development along the segments 1 and 2 in the three-terminal interconnect tree considering current density and segment length configurations: (a) Case I; (b) Case II; (c) Case III; (d) Case IV; (e) Case V; (f) Case VI.

A. Different Current Density and Segment Length Configurations

For the purpose of simulation, the metal wire structure used in our experiment has been shown in Fig. 3. The current density and segment length configurations used in our numerical simulations are shown in Table I from which we can see that the left segment length for each case is set to be shorter than the right one. Also, the current magnitude of the left segment is set to be larger than that of the right segment for each case. The stress profiles for different times shown in Figs. 9(a)–9(f) are obtained from the five-term approximation of the proposed series solution (16) and the COMSOL simulations. It can be seen from Figs. 9(a)–9(f) that the analytic solution obtained with the proposed method fits well to the results of the numerical simulations by COMSOL at every time instance.

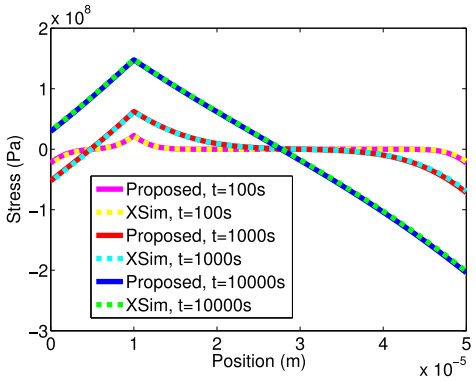

Fig. 10. The proposed analytical method compared against XSim results.

We now discuss all the cases, in which different current density and segment length configurations are set in the two line segments. In the cases I and II, the left and right segments have the same current direction. It was observed from Figs. 9(a)–9(b) that a tensile stress will be developed over time along the left segment and a compressive stress will be developed along the right segment. The tensile stress at the cathode node "a" in the left segment decreases as the current density of the right segment decreases for a fixed current density in the left segment. Generally, the left segment in the two cases is called reservoir as it has tensile stress and the right segment is called sink [37]. Fig. 9(b) shows that voids can only happen in the reservoir when the current magnitude in the sink is zero or small. However, voids can be also nucleated when the sink becomes active. This can be easily seen from Fig. 9(d) for the case when the current magnitude in the right segment is with no zero and the current direction is opposite to the left segment. In the cases III and VI, voids can be only nucleated in the left segment since the current density in the right segment is zero. The tensile stress at the node "a" increases with the length of the left segment for a fixed length of the right segment. In the cases IV and V, tensile stresses can build up at both ends "a" and "b" since the currents in the two segments are opposite in direction. Fig. 9(d) shows that voids can first form at the end "b" of the longer segment (right). On the other hand, it can be seen from Fig. 9(e) that void can also be nucleated at the end "a" of the shorter segment (left) if we decrease the current magnitude of the right segment.

To further verify the accuracy of the proposed method, we compare the proposed analytical solution with the results published in the literature on very similar structures [30], [39] in which the EM-based stress evolution in a short three-contact interconnect tree was calculated by the electromigration simulator XSim [30]. XSim is widely used to calculate the hydrostatic stress evolution in an interconnect which is assumed to be confined within diffusion barriers. In this simulation, the lengths of the left and right segments in the interconnect line are set to be $1 \times 10^{-5} m$ and $4 \times 10^{-5} m$, respectively. The width and the thickness in the interconnect tree used in XSim are set to be $0.2 \times 10^{-6} m$ and $0.38 \times 10^{-6} m$, respectively. The temperature is set to be 350°C and the current densities in the left and right segments are $-2 \times 10^{9} A/m^2$ and $2 \times 10^{9} A/m^2$, respectively. Fig. 10 shows the stress evolution

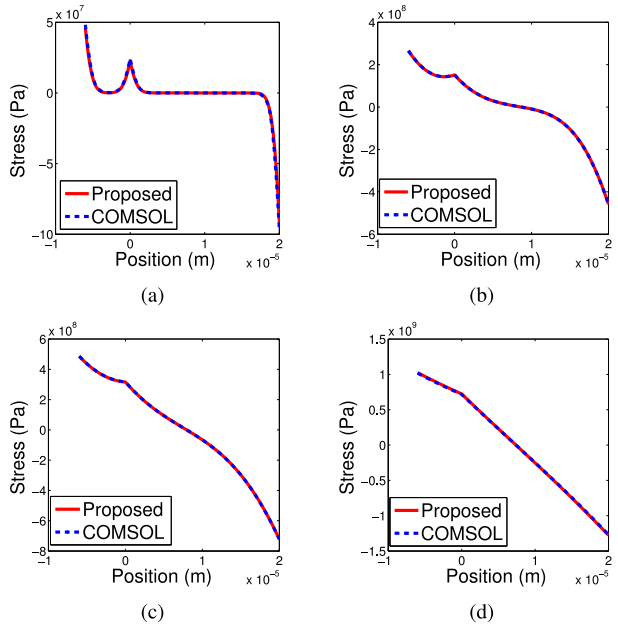

Fig. 11. The EM stress development along the segments 1 and 2 in the three-terminal interconnect tree considering time-varying temperature: (a) $t = 8 \times 10^4 s$; (b) $t = 2 \times 10^6 s$; (c) $t = 5 \times 10^6 s$; (d) $t = 4 \times 10^7 s$.

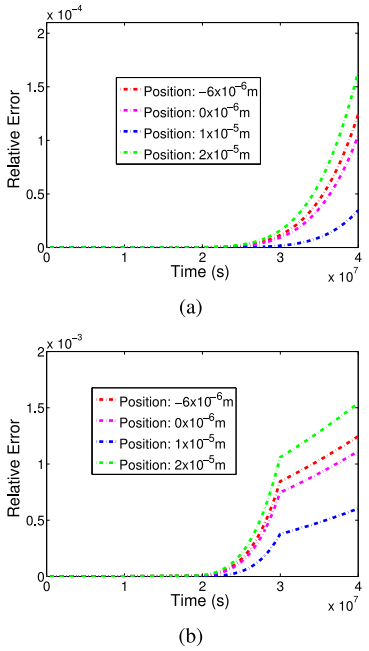

Fig. 12. Relative errors between the one-term and two-term approximations at different locations in the three-terminal interconnect tree: (a) constant temperature; (b) time-varying temperature.

calculated by XSim and using the first dominant term approximation (19)-(20) along this interconnect line at various time. We can see from Fig. 10 that XSim and the one-term approximation provide results of similar accuracy which shows the effectiveness of the proposed analytical method.

B. Dynamic EM Stress Under Time-Varying Temperature

To verify the accuracy of the new dynamic EM model, let us consider the three-terminal interconnect tree shown in Fig. 3 in which the lengths of the left and right segments are set to be $6 \times 10^{-6} m$ and $2 \times 10^{-5} m$, respectively. For our simulation, we assume that the current densities j_1 and j_2 in the left and right segments are $1 \times 10^{10} A/m^2$ and $2 \times 10^{10} A/m^2$, respectively, and we create the periodic change temperature profiles over time which can be shown in Fig. 7(a). For this case the corresponding analytic solution to the stress evolution equation (6) with time-varying temperature can be represented by (24). For comparison with the proposed dynamic EM model, we will also apply COMSOL to compute an accurate numerical solution of (6).

To illustrate the effect of time-varying temperature, we use the one-term approximation ($n = 0$) of the proposed series solution (16) and the FEA tool COMSOL to calculate the stress values during the void nucleation process. Fig. 11 shows the stress distributions under time-varying temperature along the whole length of this three-terminal interconnect tree. It can be seen from Fig. 11 that the stresses calculated by the proposed one-term approximation are in good agreement with those obtained from COMSOL. It should be noted that electrons flow from the left segment to the right segment and out of the anode end of the right segment. The slope of the stress profile will be unchanged in the interconnect tree when the stress gradually increases to a steady-state level, but it can be observed from Fig. 11 that the maximum tensile stress will be higher and will still occur at the end "a" (the cathode end) of the left segment.

C. Computational Accuracy and Convergence Characteristics

We now study the convergence behavior of the aforementioned method using the series solution (16) and we illustrate the discussion by analyzing the convergence observed in actual computations. In general, we need to compare the $(m+l)$-term approximation with the m-term approximation for arbitrary fixed nonnegative integers m and l. As we can see, Fig. 11 has shown that the dominant term of the expression (16) can match well with the COMSOL simulation results for a given current density and temperature profile for the three-terminal interconnect tree with various lengths. Therefore, we just need to compare the accuracies of the EM models employing the one-term ($n = 0$) and two-term ($n = 1$) approximations of the original series solution.

This comparison can be seen clearly from the numerical simulation results or the stress evolution process. Fig. 12 shows the comparison results between the one-term and two-term approximations for this three-terminal interconnect tree. It can be seen that the relative errors between the one-term and two-term approximations are less than 0.2% for both the constant and time-varying temperatures. Fig. 12(a) shows that using the constant temperature can lead to smaller relative errors (e.g., within 0.02%). By using more terms, the accuracy of the proposed EM model simulation results will not be significantly increased, which means that the dominant one-term approximation can achieve sufficient accuracy for practical EM analysis.

To further illustrate that the analytical series solution (16)-(17) has fast convergence, we compare the proposed

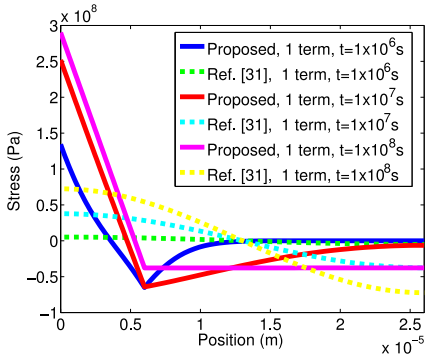

(a)

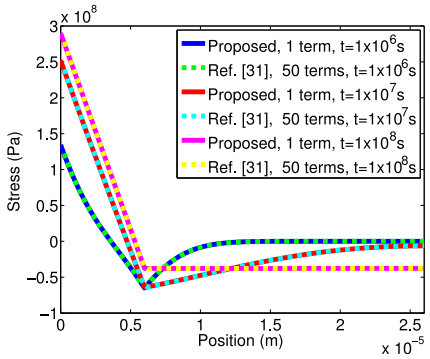

(b)

Fig. 13. Comparison between the proposed analytical method and the eigenfunction method for calculating the EM stress development along the three-terminal interconnect tree.

method with results reported in [31] for an interconnect with similar structures. In [31], the integral transform technique was used to calculate the transient hydrostatic stress represented in the form of an infinite series of eigenfunctions. The accuracy of this algorithm depends on the number of eigenfunctions used in the series solution. As discussed above, the accuracy of the proposed analytical method by using the one-term approximation is validated by numerical experiments. However, Fig. 13(a) shows that a significant error can be produced if the one-term approximation of the infinite series solution of eigenfunctions is used to calculate the stress evolution along the interconnect line. The accuracy will be improved if more eigenfunctions are used for simulation. It can be seen from Fig. 13(b) that the fifty-term approximation of the eigenfunction method can achieve the same accuracy with the one-term approximation of the series solution (16)-(17). That is to say, the analytical method proposed in this paper has faster convergence compared the eigenfunction method reported in [31]. Simulation results show that the proposed method can achieve improved performance compared with the eigenfunction method for calculating the stress evolution by electromigration of three-terminal interconnect tree.

VI. Conclusion

In this paper, we have proposed a new modeling and analysis technique for EM reliability analysis in three-terminal interconnect tree with wire segment lengths, which reflects practical VLSI interconnect architectures and interconnect layout-design techniques. By using the Laplace transform technique we have derived an exact analytical solution to the stress evolution equation for the void nucleation phase during EM of this type of interconnect tree. The effects of different current densities and segment lengths on stress evolution have been observed from the proposed analytic model. We have also developed a dynamic EM stress model considering time-varying temperature based on the obtained exact series solution at constant temperature, which reflects a more practical chip working conditions especially for multi-core and emerging 3D ICs. The numerical comparison shows that the analytical solution agrees well with the results from the finite element method based numerical analysis. It uses much less terms compared to the eigenfunction method for the same accuracy. It also agrees very well with XSim, which is consistent with the previously reported measured results.

Acknowledgment

The authors would like to thank Prof. Carl V. Thompson of MIT and Prof. Chee Lip Gan of Nanyang Technological University for providing the electromigration simulator XSim, which was used in this work for comparison.

References

[1] B. Bailey, "Thermally challenged," *Semicond. Eng.*, Dec. 2013, accessed: Feb. 16, 2014. [Online]. Available: http://semiengineering.com/thermally-challenged/

[2] V. Mishra and S. S. Sapatnekar, "The impact of electromigration in copper interconnects on power grid integrity," in *Proc. Design Autom. Conf.*, Austin, TX, USA, 2013, pp. 1–6.

[3] S. P. Hau-Riege and C. V. Thompson, "Experimental characterization and modeling of the reliability of interconnect trees," *J. Appl. Phys.*, vol. 89, no. 1, pp. 601–609, Jan. 2001.

[4] *International Technology Roadmap for Semiconductors*. (2014). [Online]. Available: http://public.itrs.net

[5] C. V. Thompson, S. P. Hau-Riege, and V. K. Andleigh, "Modeling and experimental characterization of electromigration in interconnect trees," in *Proc. AIP Conf.*, 1999, pp. 62–73.

[6] S. M. Alam, "Design tool and methodologies for interconnect reliability analysis in integrated circuits," Ph.D. dissertation, Dept. Elect. Eng. Comput. Sci., Massachusetts Inst. Technol., Cambridge, MA, USA, Sep. 2004.

[7] M. A. Korhonen, P. Borgesen, K. N. Tu, and C.-Y. Li, "Stress evolution due to electromigration in confined metal lines," *J. Appl. Phys.*, vol. 73, no. 8, pp. 3790–3799, 1993.

[8] *Failure Mechanisms and Models for Semiconductor Devices*, JEDEC Standard JEP122-A, 2002.

[9] J. R. Black, "Electromigration—A brief survey and some recent results," *IEEE Trans. Electron Devices*, vol. ED-16, no. 4, pp. 338–347, Apr. 1969.

[10] M. Hauschildt *et al.*, "Electromigration early failure void nucleation and growth phenomena in Cu and Cu(Mn) interconnects," in *Proc. IEEE Int. Rel. Phys. Symp.*, Anaheim, CA, USA, 2013, pp. 2C.1.1–2C.1.6.

[11] Z. Suo, "Reliability of interconnect structures," in *Comprehensive Structural Integrity*, vol. 8. Amsterdam, The Netherlands: Elsevier, 2003.

[12] R. G. Filippi, P.-C. Wang, A. Brendler, K. Chanda, and J. R. Lloyd, "Implications of a threshold failure time and void nucleation on electromigration of copper interconnects," *J. Appl. Phys.*, vol. 107, no. 10, pp. 1–7, 2010.

[13] M.-H. Lin and T. Oates, "Electromigration failure time model of general circuit-like interconnects," *IEEE Trans. Device Mater. Rel.*, vol. 17, no. 2, pp. 381–398, Jun. 2017.

[14] A. S. Oates and M. H. Lin, "Electromigration failure of circuit—Like interconnects: Short length failure time distributions with active sinks and reservoirs," in *Proc. IEEE Int. Rel. Phys. Symp.*, 2014, pp. 5A.2.1–5A.2.7.

[15] M. H. Lin and A. S. Oates, "Electromigration failure of circuit interconnects," in *Proc. IEEE Int. Rel. Phys. Symp.*, Pasadena, CA, USA, 2016, pp. 5B-2-1–5B-2-8.

[16] W. Li and C. M. Tan, "Black's equation for today's ULSI interconnect electromigration reliability—A revisit," in *Proc. IEEE Int. Conf. Electron Devices Solid State Circuits*, Tianjin, China, 2011, pp. 1–2.
[17] R. L. de Orio, H. Ceric, and S. Selberherr, "Physically based models of electromigration: From black's equation to modern TCAD models," *Microelectron. Rel.*, vol. 50, no. 6, pp. 775–789, 2010.
[18] J. Srinivasan, S. V. Adve, P. Bose, J. Rivers, and C.-K. Hu, "Ramp: A model for reliability aware microprocessor design," IBM Res., Zürich, Switzerland, Tech. Rep. RC23048, 2003.
[19] T. Simunic, K. Mihic, and G. De Micheli, "Optimization of reliability and power consumption in systems on a chip," in *Proc. Int. Workshop Power Timing Model. Optim. Simul.*, Leuven, Belgium, Sep. 2005, pp. 237–246.
[20] E. Karl, D. Blaauw, D. Sylvester, and T. Mudge, "Reliability modeling and management in dynamic microprocessor-based systems," in *Proc. Design Autom. Conf.*, San Francisco, CA, USA, 2006, pp. 1057–1060.
[21] V. Sukharev, "Beyond Black's equation: Full-chip EM/SM assessment in 3D IC stack," *Microelectron. Eng.*, vol. 120, pp. 99–105, May 2014.
[22] Z. Lu, W. Huang, J. Lach, M. Stan, and K. Skadron, "Interconnect lifetime prediction under dynamic stress for reliability-aware design," in *Proc. Int. Conf. Comput. Aided Design*, San Jose, CA, USA, Nov. 2004, pp. 327–334.
[23] Z. Lu, J. Lach, M. R. Stan, and K. Skadron, "Improved thermal management with reliability banking," *IEEE Micro*, vol. 25, no. 6, pp. 40–49, Nov./Dec. 2005.
[24] X. Huang, Y. Tan, V. Sukharev, and S. X.-D. Tan, "Physics-based electromigration assessment for power grid networks," in *Proc. Design Autom. Conf.*, San Francisco, CA, USA, Jun. 2014, pp. 1–6.
[25] X. Huang, A. Kteyan, S. X.-D. Tan, and V. Sukharev, "Physics-based electromigration models and full-chip assessment for power grid networks," *IEEE Trans. Comput.-Aided Design Integr. Circuits Syst.*, vol. 35, no. 11, pp. 1848–1861, Nov. 2016.
[26] H.-B. Chen, S. X.-D. Tan, V. Sukharev, X. Huang, and T. Kim, "Interconnect reliability modeling and analysis for multi-branch interconnect trees," in *Proc. Design Autom. Conf.*, San Francisco, CA, USA, Jun. 2015, pp. 1–6.
[27] H.-B. Chen, S. X.-D. Tan, X. Huang, T. Kim, and V. Sukharev, "Analytical modeling and characterization of electromigration effects for multibranch interconnect trees," *IEEE Trans. Comput.-Aided Design Integr. Circuits Syst.*, vol. 35, no. 11, pp. 1811–1824, Nov. 2016.
[28] C. W. Chang *et al.*, "Electromigration resistance in a short three-contact interconnect tree," *J. Appl. Phys.*, vol. 99, no. 9, pp. 1–7, 2006.
[29] C. L. Gan, C. V. Thompson, K. L. Pey, and W. K. Choi, "Experimental characterization and modeling of the reliability of three-terminal dual-damascene Cu interconnect trees," *J. Appl. Phys.*, vol. 94, no. 2, pp. 1222–1228, 2003.
[30] F. L. Wei *et al.*, "Electromigration-induced extrusion failures in cu/low-k interconnects," *J. Appl. Phys.*, vol. 104, pp. 1–10, Aug. 2008.
[31] X. Wang *et al.*, "Physics-based electromigration modeling and assessment for multi-segment interconnects in power grid networks," in *Proc. Design Autom. Test Europe*, Lausanne, Switzerland, 2017, pp. 1–6.
[32] F. Abraham, *Homogeneous Nucleation Theory*. New York, NY, USA: Academic Press, 1974.
[33] V. M. Dwyer, "Modeling the electromigration failure time distribution in short copper interconnects," *J. Appl. Phys.*, vol. 104, no. 053708, pp. 1–10, 2008.
[34] V. M. Dwyer, "An investigation of electromigration induced void nucleation time statistics in short copper interconnects," *J. Appl. Phys.*, vol. 107, no. 10, pp. 1–12, 2010.
[35] V. Sukharev, A. Kteyan, and X. Huang, "Postvoiding stress evolution in confined metal lines," *IEEE Trans. Device Mater. Rel.*, vol. 16, no. 1, pp. 50–60, Mar. 2016.
[36] M. E. Sarychev, Y. V. Zhitnikov, L. Borucki, C.-L. Liu, and T. M. Makhviladze, "General model for mechanical stress evolution during electromigration," *J. Appl. Phys.*, vol. 86, no. 6, pp. 3068–3075, 1999.
[37] M. H. Lin and A. S. Oates, "An electromigration failure distribution model for short-length conductors incorporating passive sinks/reservoirs," *IEEE Trans. Device Mater. Rel.*, vol. 13, no. 1, pp. 322–326, Mar. 2013.
[38] *Comsol Multiphysics*. Accessed: Jul. 15, 2016. [Online]. Available: http://www.comsol.com
[39] C. S. Hau-Riege, A. P. Marathe, and Z.-S. Choi, "The effect of current direction on the electromigration in short-lines with reservoirs," in *Proc. IEEE Int. Rel. Phys. Symp.*, Phoenix, AZ, USA, 2008, pp. 381–384.

Hai-Bao Chen (M'16) received the B.S. degree in information and computing sciences and the M.S. and Ph.D. degrees in applied mathematics from Xi'an Jiaotong University, Xi'an, China, in 2006, 2008, and 2012, respectively. He then joined Huawei Technologies, where he focused on cloud computing and big data. He was a Post-Doctoral Research Fellow with the Electrical Engineering Department, University of California at Riverside, Riverside, CA, USA, from 2013 to 2014. He is currently an Assistant Professor with the Department of Micro/Nano-Electronics, Shanghai Jiao Tong University, Shanghai, China. He has authored or co-authored over 30 papers in scientific journals and conference proceedings. His current research interests include model order reduction, system and control theory, circuit simulation, cloud computing and big data, and electromigration reliability. He was a recipient of the Best Paper Award Nomination from Asia and South Pacific Design Automation Conference in 2015. He currently serves as an Associate Editor for *Integration—The VLSI Journal*.

Sheldon X.-D. Tan (S'96–M'99–SM'06) received the B.S. and M.S. degrees in electrical engineering from Fudan University, Shanghai, China, in 1992 and 1995, respectively, and the Ph.D. degree in electrical and computer engineering from the University of Iowa, Iowa City, in 1999. He is a Professor with the Department of Electrical Engineering, University of California (UC Riverside), Riverside, CA, USA, where he is also an Associate Director of the Computer Engineering Program. He has been the Associate Director of Compute Engineering Program with Bourn College of Engineering, UC Riverside, since 2009. His research interests include VLSI reliability modeling, optimization and management at circuit and system levels, thermal modeling, optimization and dynamic thermal management for many-core processors, statistical modeling, simulation and optimization of mixed-signal/RF/analog circuits, and parallel circuit simulation techniques based on GPU and multicore systems. Prof. Tan was a recipient of the Outstanding Oversea Investigator Award from the National Natural Science Foundation of China in 2008; the NSF CAREER Award in 2004; the Best Paper Award from 2007 IEEE International Conference on Computer Design; the Best Paper Award from 1999 IEEE/ACM Design Automation Conference; Three Best Paper Award Nomination from IEEE/ACM Design Automation Conferences in 2005, 2009, and 2014; and one Best Paper Award nomination from ASPDAC in 2015. He is currently serving as the Editor-in-Chief for *Integration—The VLSI Journal*. He is also serving as an Associate Editor for the IEEE TRANSACTIONS ON VERY LARGE SCALE INTEGRATION (VLSI) SYSTEMS and *ACM Transaction on Design Automation of Electronic Systems*.

Jiangtao Peng received the B.S. degree in communication engineering from Chongqing University, Chongqing, China, in 2015. She is currently pursuing the M.S. degree with the Department of Micro/Nano-Electronics, Shanghai Jiao Tong University, Shanghai, China. Her current research interests include electromigration reliability and embedded system design.

Taeyoung Kim (S'10) received the M.S. degree in electrical and computer engineering from the University of Virginia, Charlottesville, VA, USA, in 2012. He is currently pursuing the Ph.D. degree with the Department of Computer Science and Engineering, University of California, Riverside, CA, USA. His current research interests include embedded system design, electronic design automation, reliability-aware system modeling, simulation, and optimization.

Jie Chen (S'87–M'89–SM'98–F'07) received the B.S. degree in aerospace engineering from Northwestern Polytechnic University, Xian, China, in 1982, the M.S.E. degree in electrical engineering, the M.A. degree in mathematics, and the Ph.D. degree in electrical engineering from the University of Michigan, Ann Arbor, MI, USA, in 1985, 1987, and 1990, respectively. He is a Chair Professor with the Department of Electronic Engineering, City University of Hong Kong, Hong Kong. He was with the School of Aerospace Engineering and the School of Electrical and Computer Engineering, Georgia Institute of Technology, Atlanta, GA, USA, from 1990 to 1993, and with the University of California, Riverside, CA, USA, from 1994 to 2014, where he was a Professor and served as a Professor and the Chair with the Department of Electrical Engineering from 2001 to 2006. He has authored several books, including the books entitled *Control-Oriented System Identification: An H-Infinity Approach* (Wiley-Interscience, 2000; with G. Gu), *Stability of Time-Delay Systems* (Birkhauser, 2003; with K. Gu and V. L. Kharitonov), and *Towards Integrating Control and Information Theories: From Information-Theoretic Measures to Control Performance Limitations* (Springer, 2016; with S. Fang and H. Ishii). His main research interests are in the areas of linear multivariable systems theory, system identification, robust control, optimization, time-delay systems, networked control, and multiagent systems. Dr. Chen was a recipient of the 1996 U.S. National Science Foundation CAREER Award, the 2004 SICE International Award, and the 2006 Natural Science Foundation of China Outstanding Overseas Young Scholar Award. He served on a number of journal editorial boards, as an Associate Editor and a Guest Editor for the IEEE TRANSACTIONS ON AUTOMATIC CONTROL, a Guest Editor for the *IEEE Control Systems Magazine*, an Associate Editor for *Automatica*, and the Founding Editor-in-Chief for the *Journal of Control Science and Engineering*. He is currently an IEEE Control Systems Society (CSS) Distinguished Lecturer and serves as an Associate Editor for *SIAM Journal on Control and Optimization*. He was a member of the IEEE CSS Board of Governors in 2014 and has been serving as IEEE CSS Chapter Activities Chair since 2015. He is a Fellow of AAAS and IFAC, and a Yangtze Scholar/Chair Professor of China.